Energy conversion modeling on the intrinsic persistent luminescence of solids via energy transfer paths between transition levels

Bolong Huang and Mingzi Sun

Department of Applied Biology and Chemical Technology, The Hong Kong Polytechnic University, Hong Hum, Kowloon, Hong Kong SAR, China

Email: bhuang@polyu.edu.hk

Abstract

The energy conversion model has been established for the intrinsic persistent luminescence in solids with related to the native point defect levels, formations, and transitions. In this work, we show how the recombination of charge carriers between different defect levels along the zero phonon line (ZPL) can lead to the energy conversions supporting the intrinsic persistent phosphorescence in solids. This suggests that the key driving force for this optical phenomenon is the pair electrons hopping between different charged defects with negative-U_{eff}. Such negative correlation energy will provided sustainable energy source for electron-hole further recombine in a new cycle with a specific quantum yield. This will help us to understand the intrinsic persistent luminescence from the aspect of native point defect levels as well as the correlations of electronics and energetics.

1. Introduction

Persistent luminescence materials are solids characterized by long-lasting emission of light after the external irradiations of UV or high energy X-ray excitations [1-4]. The optical band gaps of these materials are usually from 3 to 12 eV differently, and their phosphorescence properties are mostly modulated by rare earth dopants in purpose of illumination time extension, intensity enhancement, or color of emission (wavelengths)[5-12]. But more unusually, there have been some of the ordinary oxides or solids have presented an intrinsic persistent phosphor behavior that leaves without any support of extrinsic dopants like rare earth ions (RE^{2+}, RE^{3+}). Recently, some oxides have even exhibited an upconverted persistent luminescence without any extrinsic doping[13]. The explanation for this properties has so far been sought an conventional energy transfer in terms of upconverted energy levels by 4f orbitals of rare earth ions combining an electronic down-conversion recombination with holes before emission[14].

The emission of the conventional persistent luminescence solid usually relies on an activator acting by a sort of extrinsic $RE^{2+/3+}$ such as Eu^{2+}, Ce^{2+}, Yb^{3+} or Er^{3+}, which follows the inter excited orbital levels of energy transferring model, where the levels of secondary RE dopants aligned in the optical fundamental gap are similar to that of the energy traps for holding excited charge carriers. The consequent intensity and time of persistent luminescence are determined on the concentrations and depths of charge traps. The excited electrons are de-excited back to the activators to recombine the holes from conduction band minimum (CBM) owing to the thermal perturbation (~k_BT, k_B denotes the Boltzman constant). The relative energy will be released in terms of photons of luminescence.

2. Prerequisite for energy transfer and conversion modeling

With increasing production of intrinsic non-metal/RE ion activated persistent luminescence, mechanisms related to the energy transfer and conversions are required as the prerequisite for guiding high-throughput experimental synthesis and modulations.

2.1 TSL or DLTS?

Thermal stimulated luminescence (TSL) measurements have been useful to describe the trap depths away from the CBM based on an Urbach empirical equation [8, 12]. Leverenz and Ghosh et al have both summarized detail equations on duration time of persistent luminescence with related to the trap depths [15, 16]. However, this has less information on how the electrons have been transferred upward to the CB from the valence band maximum (VBM), moreover, the traps levels and related defect formations will be changed as the temperature varied. Thus, the TSL spectra usually demonstrate a widely distributed “band” where is the multi-centers of thermodynamically stimulated luminescence by recombination of charge carriers. This also leaves us a question that TSL usually describes electrons down-conversion luminescence, the holes can be also accounted as dominant charge carriers implemented in the persistent luminescence that indeed cannot shown by TSL. In which case, there is a model that has a way of describing the upconverted persistent luminescence in either terms of electrons- or holes-dominant transport? (Note in the later part, we will interpret the thermally temperature-induced phonons will influence the energy transfer.)

Above the TSL is a tool for measuring the trap depth of luminescence samples. Similarly under the framework of thermal emission properties, another different technique introduced

here is called deep-level transient spectroscopy (DLTS) originally developed by Lang [17, 18], which has been already mature in observing a wide variety of traps in semiconductor or wide band gap solids with high sensitivity and rapid frequency scanning speed. In addition, one can measure the activation energy, concentration profile, and electron and hole capturing cross sections for each intrinsic trap or doping impurities. The technique is presented with either a simple theoretical analysis for the case of exponential capacitance transients or the more advance density functional theory (DFT) calculations with self-consistent orbital corrections. It not only presents the trap depth, concentrations, positions in temperature, but also reflect the defect thermodynamic transition level (TTL) between different intrinsic charge states[19, 20].

Here we show that the conventional upconversion mechanism between 4f levels of rare earth element alone cannot account for this phenomenon and that it is due to an unusual charge alternation process and lead to an energy transfer between donor-acceptor bands induced by time-accumulated donor-acceptor pairs of charge carriers, resulting in a large time decay constant for phosphorescence of these materials. So, we firstly divide the ideal energy transfer scheme with different relaxation time for electrons at the energy levels: one is the transient state transitions, and the other is long relaxation life-time without assistance of the multi-phonons. In the conventional fluorescence energy transfer such as non-radiative FRET model, the excited electrons at the different transition levels are usually presenting a transient state of which the activation time is evidently less than 10^{-8} s. The external excitation source is usually the pulsed-laser with time-width less than 10^{-9} s or within the range of 10^{-12}~10^{-9} s. The time-width of emission by the de-excitation between inter-transition-level is also rather short within the magnitude from 10^{-9}~10^{-6} s.

As is well known, the persistent luminescence solids can accept wide range of external stimulation and are capable to accept many manners of high energy irradiation to excite the electrons to the localized defect levels with long relaxation life-time. Therefore, it is necessary to propose the energy transfer model with a transition scheme independent to the external temperature environment and non-radiative phonon emissions.

2.2 Rejuvenate the Utilization of FRET

Another question is whether the energy transport through the lattice and transfer between different ions is being carried out by real (“freely mobile” electrons) or non-real entities. Leverenz has discussed a class of quantitative models that the energy transport being actualized by “free” electrons [15, 21]. It is probable that most of the energy transport in phosphors can be understood by excited “free” electrons between different localized levels of intrinsic defects or impurities. But, the problems of energy transport in solids are complicated and most of the phosphor host solids are insulators with wide band gaps. To prevent the incompatible issues on electronic conductions in the persistent luminescence, Föster type non-radiative resonant energy transfer (FRET) model (or fluorescent resonant energy transfer from literatures) [22] can be available to assist the exploration on the mechanism of phosphorescence, which has been also being extensively derived by the work of Auzel to interprete the anti-Stokes type energy upconverted luminescence[23, 24]. This FRET energy transfer model requires the co-existence of the sensitizer and activator ions (S-A pairs) in the host lattice. Note that, in most of the persistent luminescence solids, the efficiency, intensity, and luminescence time are determined by the intrinsic traps or impurity levels dominantly instead of distinguishable well-defined S-A pairs. At the meanwhile, the mechanism of the

persistent luminescence especially to the long-time emission behavior is quite different to the upconversion.

2.3 Why defects?

The mechanism of the persistent luminescence exists in certain class of crystal solids because of the nearly constant energy conversion circulation [25, 26]. To drive such energy conversion, we need to understand how the photo-excitation interact the defect and how the defects change between different charge states.

As we know, the native point defects are of great importance in controlling the creation and annihilation of free or localized (bounded) charge carriers in the solids. The electrical and optical properties of solids are actually dominated by their point defects. The defect study has motivated us a strong intention in predicting their electron transport [27-29], electrical conduction[30-32] and luminescence properties [25, 33], and explaining the experimental observations. There are three main interesting point for defects in the solids are: (i) the defect formation energy $H(\mu, E_F)$ is a function of the Fermi energy (E_F) and chemical potential μ of the solid components. The formation energy decides the defect or doping concentration reachable in the solids at a given temperature as well as the E_F in equilibrium. (ii) The thermodynamic transition energy, is the energy E(q, q') required to ionize the defect or dopant center from charge state q to q'. It is also called donor or acceptor transition energy which presents the ability of the defect or dopants to produce the free charge carriers at a specific E_F or a given temperature. (iii) The charge localization of the defect or dopants that show localization of carriers. To our knowledge, the acceptors in oxides often introduce hole states localized on single oxygen but wrongly described by lower level of functional chosen in DFT calculation, and have recently correctly confirmed the localization by more accurate calculations [34-36].

This paired opposite charged defects is required to be the lowest formation energies in total within the host lattice. This can attribute to the Schottky and Frenkel (anion-Frenkel) type defects. They present in neutral by consisting of two opposite charged defects. Schottky defect has one cation vacancy and one anion vacancy while the anion Frenkel defect has one anion vacancy and one anion interstitial defect. The charge transition occurs between the sub-defect sites of these pair defects and depends on which one forms with the lower energy in the host lattice.

Huang et al have studied that these pair intrinsic defects can be formed by the temperature perturbation/fluctuation [31, 32]. In our previous studies, the neutral Schottky defects does not provide any gap states, but become electrically active when an excess charge exchanges, while the a-Fr defect usually give relatively shallow acceptor-like level in the host lattice. Their mobilities migrating in the host lattice determine the time scale within a range of 10^{-3}~10^{-6} s. This is largely consistent with the electronic dynamics response of phosphors. The reason we focus on these types of defects is that their recombination would release an energy which evidently match the energy of photon released in scale during the process of persistent luminescence. This can be explained by a concept called negative effective correlation energy (negative-U_{eff}) proposed by Anderson[37, 38], Mott[39-42], and Davis[43], in explaining the electron-lattice coupling by defect charge reaction in many both crystalline and non-crystalline solids [44-47].

The charge alternation pairs (CAP) among the intrinsic point defects of host lattice are bounded excitions and can be co-stabilized in either short or large crossover distance within the lattice by electronic Coulomb potentials. With the negative effective correlation energy (negative-U_{eff}), the hopping of two electrons between different energy transition states can overcome the Coulomb repulsive potential through the localized levels of the bounded pairs and lock-in their life-time within the equivalent scales. Meanwhile, the transition is implemented along the zero-phonon-line of the electronic structures from the host lattice. Therefore, the defects states in the solids play significant role in interpreting the electronic transitions for assisting the energy transfer through the corresponding correlated pairs. This also leads to different defect structures and reactions, which account for the orders of magnitude difference in their decay time and intensity.

2.4 Existing energy transfer mechanism

The existing answer is that the energy transfer (energy released from donor- to acceptor-level) migrates to support the non-linear optical excitations in upconversion luminescence given by the dopant of $RE^{2+/3+}$. This largely requires the donor-like traps stays below the CBM and acceptor-like traps above the VBM, meanwhile, they are shallow traps which mean the donor traps are always higher than the acceptor traps. On the other hand, it also requires the transferred energy is large enough to support energy transfers between of 4f levels. However, the Romanov et al showed that even the updoped ZnO presented an upconverted persistent luminescence showing the related energy transfers without any RE activators [48, 49]. Moreover, Buyanova et al observed that an efficient upconversion persistently existed in ZnO which is dominantly contributed by the native point defects such as zinc vacancy (V_{Zn}) [50] via either two-step two-photon absorption (TS-TPA) or TPA.

Moreover, many materials present intrinsic persistent luminescence without any doping. Similar phenomenon has been also observed in the other materials like hafnium oxide (HfO_2) [2, 51], erbium sesquioxides (Er_2O_3) [13], and aluminum nitride (AlN) [52]. According to the experimental reports, these undoped solid materials have all presented afterglows. We summarized this property is not due to its own unique electronic like 4f-5d or 4f-4f transitions in Er_2O_3 since the experimentally reported the persistent luminescence emission bands appear to be the same for different Ln_2O_3 (Ln=Pr, Nd, Sm and Er) [13, 53]. Hence, neither existing experiment not modeling adequately explains the origin of the upconverted persistent luminescence.

3. Calculation setup

As is well known, the stable lattice structures have been observed for yttrium oxide (Y_2O_3), which is bixbyite (C-type, Ia-3) [54]. For the HfO_2, we elucidate the luminescence mechanism by using the cubic lattice within symmetry group of *Fm-3m* (fluorite-type).

The lattice relaxation of Y_2O_3 at the ground states is remained at the PBE or PBE+U level by CASTEP code [55], since PBE has been proven to be reliable enough for structural relaxation and internal geometrical optimization of 4f- or 5f-level based solids [56], independent to the choice of pseudopotentials. It was also showing that the pseudopotential based f-level solids have a minor or negligible variation on the lattice parameters by DFT or DFT+U [31-33, 57-59]. However, the empiricalchoice of the Hubbard U parameters actually induces residue of self-energy of localized orbitals for electronic structures [31-33, 57-59].

We decided chose five orbital components that is (4*s*, 4*p*, 4*d*, 5*s*) to represent the valence states of the Y atom, and (5*s*, 5*p*, 5*d*, 6*s*) for Hf atom. We chose norm-conserving pseudopotentials as this theoretical treatment can reflect all-electron-like behavior for valence shells with overlapping integral factor of |**S-matrix**|=1 [60, 61] by using OPIUM code with RRKJ optimization method [62]. Each of the valence orbital projector has been augmented by a "tailor-made" the norm-conserving pseudopotentials within the KB (Kleinman-Bylander) framework [63]. For the mixed valence heavy ion system, the non-linear partial core corrections [64] has been used [31]. In addition, we chose the scalar relativistic averaging scheme [65] for local hybridization of semicore 4f-5d orbitals and relativistic effect of Y^{3+}.

For the plan-wave basis set, we set the cutoff energy to 750 eV to expand different valence orbital of Y^{3+} and Hf^{4+} as well as the strongly localized states induced by 2p orbitals of O^{2-}. To guarantee the convergence and avoid the charge-spin out-sync sloshing, we uniformly chose the ensemble DFT (EDFT) method of Marzari et al [66]. For the k-point sampling mesh, we chose a grid of 2 × 2 × 2 for all related reciprocal space integration for supercell of Y_2O_3 and HfO_2. By the above setting, the convergence tolerance of total energy calculations is set to no higher than $5.0\text{x}10^{-7}$ eV per atom, and the optimizations of Hellmann-Feynman forces in defect calculations are accomplished to lower than the level of 0.01 eV/Å. The Baldereschi special k-point (¼, ¼, ¼) [67] with Gamma-center-off was also self-consistently selected for energy comparison. Regarding the geometry relaxation, the algorithm based on Broyden-Fletcher-Goldfarb-Shannon (BFGS) method has been used through all bulk and defect supercell calculations.

We chose the rotational-invariant type DFT+U method developed by Anisimov [68]. To reduce the influence of the localized hole states produced by 2p orbitals of O sites, the self-consistently determined Hubbard U potentials is also applied on the O-2p orbitals, which have been reached a consensus [58, 69-71] in many oxides materials. Thus, it is necessary to consider both self-energy corrections on f- and p-orbitals for rare earth oxides[31-33].

For the equation used for defect formation energy calculations at different charge states (*q*), the overall supercell was established and remained constantly based on the ground state relaxed primitive cell, which is for reducing the side-effect of enthalpy changes by cell variations. The formation energy of a targeted defect (H_q) at the specific charge state *q*, can be described as a relation of the positions of Fermi energy (E_F) and the chemical potential $\Delta\mu$ of species of defects α , which is shown as follow:

$$H_q(E_F,\mu) = \left[E_q - E_H\right] + q\left(E_V + \Delta E_F\right) + \sum_\alpha n_\alpha\left(\mu_\alpha^0 + \Delta\mu_\alpha\right), \quad (1)$$

We see that the E_q and E_H are the total energy of a relaxed defective lattice with charge state *q* and an ideal lattice of host materials at the ground-state, respectively, the ΔE_F is the change of Fermi energy with respect to the valence band maximum (VBM, E_V=0), and n_α is the number of atoms of element α chosen as targeted defect sites, finally the μ_α^0 is referenced chemical potential, based on the well-established methodology provided by the work of Zunger et al [72].

4. Results and Discussion

Previously we suggested that the native defect induced upconverted persistent luminescence arises from an electron-hole excitation along the zero-phonon line (ZPL) of

various charge complementary defects through a series of charged defect reactions [25, 26]. This arises because the importance of native point defects in solids in controlling the creation and annihilation of charge carriers has long motived a strong interest in predicting their electrical and optical properties[20, 27-30]. In some systems with evident electron-lattice coupling, the local-to-medium range disorders lead to a lattice relaxations induced by a class of native point defects with negative effective correlation energy (negative-U_{eff}) [28-30]. The related defect reactions in chemistry will consequently be exothermal that pumps up electrons back to excited states with a specific yield. We verify this here using simple model.

4.1 CAP model

Here we propose a charge alternation pair (CAP) model to describe the mechanism of native defect related persistent luminescence. Figure 1 illustrates the proposed mechanism of upconverted persistent luminescence of a compound with both cases of shallow and deep donor-acceptor pair traps. We take the up-left panel as an example of n-type dominant charge carriers of persistent luminescence. The black solid arrow shows a captured electron q start to move from the lowest neutral acceptor-like native defect center A^0 where an excitation occurred. Note the D^0 is the corresponding lowest neutral donor-like intrinsic trap. The purple crossover solid dot represents a charge alternation point that both acceptor- and donor- like defects centers have the same Gibbs free energy, i.e. defect formation enthalpy, $H_A(q)=H_D(q)$, which means a point that the q is hopping from charged A^- to D^+ without any electron-phonon coupling in theoretical view. The local lattice distortion provides a supports to an alternation process that happens along ZPL without any phonon obstructions or non-radiative transition. This q will recombine the hole h at A^0 indicated by blue dashed arrow and release photons with an energy of *hv*. The whole process of charged defect reactions is listed as follows:

$$storage: (a-Fr/STK) \rightarrow (D^0 + A^0)\ or \begin{cases} A^- - q = A^0 \\ D^+ + q = D^0 \end{cases} (q = e,\ with\ external\ excitation,\ E_X) \quad (2)$$

$$release: (D^0 + A^0) \rightarrow (D^+ + A^-) + U_{eff,1} \rightarrow \cdots \rightarrow (D^{n+} + A^{n-}) + U_{eff,n} \quad (3)$$

where the point that occurs charge alternation is showing by Eq. (2) as the D and A defects proceed a charging effect by external excitations in energy of E_X as external UV irradiation shown in Figure 2. As we know, in the solid, the types of intrinsic point defect that responsible for the energy transfer in the persistent luminescence are divided by donor and hole traps respectively. Therefore, we accordingly classified them into D and A, with superscript 0 as charge q=0, + for q=+1, - for q=-1 and so on. With this model, we can setup the code and modeling in our DFT calculations that, only one single unit charge can be allowed to interact with only one photon. This indicates from the energy transition level calculations that the number of effective electrons participated in the energy transfer means the number of photons that absorbed or transferred for further cycle of the persistent luminescence. In the above Eq. (2), a-Fr denotes the anion-Frenkel pair defect and STK represents the Schottky-type pair defect the host lattice.

We see from Figure 1 that the n-type charge carriers assisted upconverted persistent luminescence is divided into two possible chemical potential limits for defect formations, the cation- and anion- rich. This may lead to a difference in formation energies of A and D defects, which arises from the slight off-stoichiometry. Although the required formation energy is high for A^0, the relative external excitation will assist it to capture an electron q

from the host lattice. The charge q will flow from higher chemical potential defect onto the lower site in either way of hopping or radiation (luminescence). The upconversion is the process that transports the charge carriers with excited energy to climb from lower chemical potential defect site to a higher site under an external UV photon-irradiation. The persistent luminescence is the process that the charge recombines with the opposite charge at the original defect site continuously supported by an energy transferred by the upconversion along the ZPL. Due to the realistic factors such as lattice antisites, impurities, high-temperatures etc., the upconversion will be obstructed by non-zero phonon coupling that deviate away/off the ZPL. This explanation is also valid for the p-type assisted upconverted persistent luminescence. The difference from the case of n-type is that both A and D are deep defect traps that close to the CBM and VBM respectively. We see that the point of charge alternation stays outside of the area of charge recombination due to the above difference. The charged defect transition levels denoted by the E_F positions are the differences of capabilities of charge captured.

The A defect site usually has excess electrons that is un-paired, and prefers to capture an excess electron to be spin-paired. However, there will be a Coulomb repulsive potential to the electron to transfer since the A is multi-electron center. The electron will overcome the Coulomb repulsion with assist of local distortions of defect lattice. This process has an evident electron-lattice coupling effect. Therefore, the negative-U_{eff} lattice distortion provides continuous energy to pump electrons to excited states as a time accumulated D band and recombine the holes at the A band along the ZPL. Note, the crossover distance between D and A is large enough, they may not be a Schottky (STK) or a-Fr pair defects. With lattice local dynamics and distortions, these defects will movable from separate apart to closely contact.

The central concept of the intrinsic upconverted persistent luminescence is the electron-acceptor recombination along the ZPL. This actually arises from a pair of electrons hopping which is relying on the existence of electron-lattice coupling with negative-U_{eff}. Such pair of electrons is sitting on a pair of D and A sites with different charge states. So the pairing of these two electrons is indeed the charge recombination of D and A sites. It exists on account of the indirect electron-electron exchange-correlation interactions mediated by the nuclei of the atoms in the host lattice. The electronic excitation along the ZPL is the transport of electron between different sites that holds different energy but without any lattice relaxation or coupling in total. Since that local distortion is rich in positive charge, and the energy gained by this distortion is large enough to overcome the energy barrier of Coulomb repulsion when two electrons approach together. Hence, there is a virtual attraction between the two electrons, and they move together as a pair in equivalent to charge recombination of D and A sites following the attractive chemical trend. The alternation of the charge between D and A sites are actually the pairing of the two electrons (i.e. CAP model introduced above). The conceptual reaction is shown as follows:

$$\begin{cases} D^0 - e = D^+ + \Delta_1 \\ A^0 + e = A^- - \Delta_2 \end{cases} \tag{4}$$

$$\Delta_1 - \Delta_2 = (n_1 - n_2)\, E_{phonon} \ , (E_{phonon} = \hbar\omega_0) \tag{5}$$

Based on the above Eq. (4) and (5), for any isolated CAP model within a closed ZPL cycle path in the transition level diagram, the electron moves from D to A site as paring effect the lattice induced the number of phonons are different as shown in Δ_1 and Δ_2 in the Eq. (4) and

(5). The electron gain the energy of n_1E_{phonon} from the lattice when is donated, while the electron release the energy of n_2E_{phonon} when is captured by A center. The ω_0 shown in Eq. (5) denotes the eigen-frequency of the host lattice during the energy transfer for the persistent luminescence.The CAP model related charge recombination for persistent luminescence occurs when $(n_1-n_2)\approx 0$, where denotes the path of D-A recombination, which means the ZPL.

The electron described by CAP model accordingly undergoes less phonon scattering than an individual electron travels through the host lattice of a solid. This arises because the distortion caused by one electron can attract back the other electron once it is scattered out of its path in a collision. Because the CAP is stable against scattering, it can carry charge freely through the solid [45], and thus give rise to super-long time decay phosphor (persistent luminescence) after external UV photo-irradiation. The local distortion might be disrupted by thermal motion of the ions in the solids, so the recombination along the ZPL very efficiently occurs at the relatively low temperature.

Figure 3 summarized current solids that have intrinsic persistent phosphors. By converting the emission wavelength (λ nm) into the photon energy (E=hν eV) by E=1239.85/λ (eV), the y-axis is our calculated photon energy and the x-axis is the experimentally observed emission photon energy. The linear correlation coefficient r shows the linear relationship with 0.96, which confirms the validity of our theoretical model. We have selected Er_2O_3, HfO_2, Y_2O_3, ZnO, CaS, and CaZnOS as samples to testify the validity of our model. The photon energy calculated on Er_2O_3 has been previously introduced in our work [26]. The Er2O3_1, Er2O3_2, Er2O3_3 are denoting the peak positions calculated by our method consistent with experimental observations [13] in terms of photon energies. Similarly, the CaZnOS system have been extensively introduced and detailed discussed by us and collaborators in forms of native point defects [73] and transition metal doping [74] for interpreting the different luminescence scenarios observed.

The results show that the CaS has slightly deviated from the diagram which arises because the sample of CaS usually contains sodium impurity [12, 16]. As to our CAP model, the persistent phosphor with twin-peak is consistent to the experiental results summarized by Ghosh et al [16]. The Schottky pair defect in ZnO wurtzite lattice has lower formation energy than the anion Frenkel pair defect. Based on the Figure 1 and 2, the source of energy conversion for the intrinsic phosphorescence is the transition between V_O and V_{Zn}. They are both negative-U_{eff} center for donating and capturing electrons respectively. Our simple GGA+U calculation shows that the calculated photon emission energy is about 2.34 eV, which is close to the experimentally reported intrinsic phosphor emission photon energy of 2.14 eV (580 nm in wavelength)[48, 49]. The Hubbard-U parameter is self-consistently determined through previous established methodology [33, 59].

4.2 ZnO

First, let's take the transparent semiconducting oxides, ZnO, as an example. Recently, experimental works by Wang et al show that the ZnO nanowire (NW) has a large enhanced efficiency in stimulated emission by piezo-phototronic effects [75, 76]. Their emission spectra on the different luminescence center and excitations show that the defective emission of NW-ZnO is centering at 580 nm, and the intensity is monotonically dependent with the external piezo-electrical field. At the meanwhile, Yan's group has remarkably shown that the multi-scaled and multi-dimensional ZnO naomaterials have also presented the intrinsic green emission higher than 510 nm in their controllable morphological experiments[77]. Later, the

hierarchical type ZnO system has the intrinsically wide 567 nm orange emission. It is interesting that, an after-glow (persistent phosphorescence) has also been observed in the ZnO systems reported recently by Baranov et al [48, 49], in which the persistent luminescence emission spectrum peak is centering at the energy of 2.2 eV (~580 nm) for photon emissions.

From literature review, there have been a variety of interpretations on the intrinsic emission of ZnO systems. For instance, for the intrinsic green and emissions of ZnO, it was firstly interpreted by the contribution of singly occupied oxygen vacancy (V_O, O-vacancy) with photoexcited holes at the 510 nm [78]. Similarly, for the intrinsic orange green emission, it has been also attributed to the transitions between photogenerated holes and singly ionized V_O [79, 80]. On the contrast, more accurate theoretical calculations on multiscaled ZnO show the V_O site has either doubly or none occupied electrons endowing with relatively large negative effective correlation energy (negative-U_{eff}) with magnitude of U_{eff}= -2.1 eV [20, 34, 81]. Moreover, recently detailed mechanism analysis combining with control experiments under cryogenic temperature demonstrates such intrinsic luminescence centering around the photon energy of 2.4 eV (510~580 nm) is contributed by defect complex like Schottky pair defects (e.g. V_{Zn}-V_O) instead of single V_O [82]. As shown in Figure 3 that, the experimentally reported the phosphorescence in ZnO system gives the energy emission by photons of 2.14 eV or 580 nm in wavelength. From our calculation, we confirm that the Schottky (STK) type defect with combination of V_O+V_{Zn} responsible for the energy transfer in electronic transition between the emission levels. The calculated photon energy is 2.34 eV through the thermodynamic transition level (TTL) calculation by DFT method. The transition undergoes the ZPL between the V_O and V_{Zn} with transitions of (0/2+) and (2-/0) respectively, which is the energy level between E_V+3.02 eV and E_V+0.67 eV in ZnO system, where the E_V denotes the position of the top of VBM of ZnO. Moreover, the Gibbs free energy of the defect complex suggest the combination of V_O+V_{Zn} in close-contact has the neutralized energy of 3.74 eV per pair defect, or 1.87 eV per defect site, independent to the Zn-rich or O-rich chemical potential limit.

From our previous work, similar system like CaZnOS has similar intrinsic phosphor due to the pair defects of Schottky defects (V_{ZnO} or V_{CaZnOS})[73]. It has been once proposed by Ghosh et al [16] that some typical solids for persistent luminescence like alkaline sulfides can be assigned a discussion on the trend of bonding iconicity. However, some novel synthesized nanomaterials such as covalently bonded AlN helices also presented a persistent long afterglow that account for the native point defects only, recently observed by Song et al[52]. Therefore, the new mechanism we introduce and discuss here is yielded beyond the type of bonding character of the host lattice.

4.3 CaS

How does the defect reaction in Eq. (3) proceed with long-lasting constant rate of energy conversions in persistent luminescence? We preliminary showed our energy conversion chain reactions (ECCR) diagram in terms of a-Fr pair defects. Here we further illustrate this diagram in terms of STK defect in CaS as an example. As we know, the vacancies are the most common defects in the crystal solids, particular to the vacancies of anions and cations. In previous work, we identified the typical native point defects in CaS are vacancies (both S and Ca) and Schottky (STK) pair defect responsible to the experimental reported persistent luminescence spectrum[25]. The STK is a type of common stoichiometric defects that form in pairs of anion and cation vacancies within the ionic crystal solids. As we know in CaS, the

far-away V_S and V_{Ca} are actually independent to each other, but the STK will form when they (V_S+V_{Ca}) move or form closely adjoining to each other in the lattice. Thus, in detail description based on our previous work, it is the energy conversion dynamics circulating among the V_S, V_{Ca}, and STK pair defect. However, it is unclear to the internal charge distribution of the neutral STK (STK^0). So here we only ideally treat these defect complexes that can be composed of V_S^0+V_{Ca}^0, V_S^++V_{Ca}^+, or V_S^{2+}+V_{Ca}^{2+}.

Figure 4 shows the process of the decomposition of Schottky (STK) pair defects by the excitations of photoirradiation, and the post evolutions of the different charge states of the defects. As shown in Figure 2, with the UV photo-irradiation, the STK defects in CaS are all excited to a meta-stable state that split into the separate anion and cation vacancies with a relative small crossover distance. These anion-cation vacancy pairs (i.e. CAPs) are firstly generated within the neutral states, as in the host materials the neutral cation vacancy has relatively small formation energy. Following the charge variations, the neutral CAPs transform into the singly charged CAPs as (V_S^+ + V_{Ca}^-), and further doubly charged state (V_S^{2+} + V_{Ca}^{2-}). This process comes along with two energy emission in terms of photons. The energies of photo emission are collected by the adjacent STK defect pairs with specific possibility due to the phonon assisted during the energy transfer through the host lattice vibrations (actually it is the ECCR advance yield). In the second round circulation, a number of STK^0 nearby the CAPs of the previous circulation are further decomposed into neutral CAPs. Then the energy conversion is further sustained in terms of energy release and collections. Such chain reaction carries forward based on the approximation of low level of electron-phonon-coupling effect. Meanwhile, the new STK defects generated by emitting photon energies from the last reactions has nearly fix rate as it possibly determined by the intrinsic structural feature of ionic crystal solid like CaS. As we known from the transitions in Figure 1, these transitions denote the levels transit without any participant of phonons ideally, as demonstrated in following Eq. (6).

$$\begin{cases} V_S^0 + V_{Ca}^0 \rightarrow V_S^+ + V_{Ca}^- + Q_1 \\ V_S^+ + V_{Ca}^- \rightarrow V_S^{2+} + V_{Ca}^{2-} + Q_2 \\ STK^0 + Q_3 \rightarrow V_S^0 + V_{Ca}^0 \end{cases} \quad (6)$$

4.4 Y_2O_3

The yttrium oxide (Y_2O_3) has been also reported that there is an intrinsic phosphor found by Lin et al [83] via Pechini-type sol-gel synthesis method. It has been remarkably reported that such powder sample was being observed without any metal or RE assisted as activators. The intrinsic phosphor luminescence is reached to the bluish-white color, especially with longer wavelength of UV light for irradiation.

Our calculation by CAP model shows the emission photon energy is 3.00 eV which is 413 nm in wavelength. This is very close to the experimental 416 nm (2.98 eV) in phosphor emission spectrum, in which the color is bluish-white. Through our calculation, we found that the a-Fr has relative low formation energy similar to previous conclusions in CeO_2 system, as the Y_2O_3 can be seen as distorted fluorite structure. When the a-Fr separates apart by external excitation, the V_O and I_O will follow from neutral state to the singly charged with opposite symbol. The electrons trapped by the V_O will hop on to the hole-trap centers for recombination through following reactions. Similar finding has been also verified in the

intrinsic upconverted persistent luminescence in non-doped Er_2O_3 within anti-ferromagnetic phase previously [26].

The thermodynamic transition levels and the single-particle levels of native point defects with different intrinsic charge states in the Y_2O_3 have been calculated and summarized in the Figure 5 and Figure 6. In this calculation, all of the intrinsic defects have been considered, and we finally chose the representative point defects with relative low formation energy, such as yttrium interstitial (Y_i), yttrium vacancy (V_Y), oxygen vacancy (V_O), as well as the oxygen interstitial (O_i). The V_O site in Y_2O_3 has the lowest formation energy of 0.58 eV among the all neutral intrinsic defects under the Y-rich (O-poor) limit, while 7.36 eV for Y-poor (O-rich).

Figure 5 shows that the thermodynamic transition level (TTL) of (0/+) and (+/2+) at E_V+4.68 eV and E_V+3.95 eV (E_V denotes the position of the VBM), which are correspondingly to the excitation wavelength of 265 nm and 314 nm respectively by external UV irradiation. The V_O in Y_2O_3 is found to be a positive-U_{eff} center (+U_{eff}), which is similar to the results in Er_2O_3 from our previous work, which means the defect reaction of $2V_O^+ \rightarrow V_O^0 + V_O^{2+}$ is endothermic process and the electron on the V_O^+ site can be stably existing through the host lattice with a long life-time. The defect reactions on Y_i site are all showing a negative-U_{eff} effect following reactions of $Y_i^+ + Y_i^{2+} \rightarrow Y_i^0 + Y_i^{3+}$; $3Y_i^{2+} \rightarrow Y_i^0 + 2Y_i^{3+}$; and $6Y_i^+ \rightarrow 4Y_i^0 + 2Y_i^{3+}$ with U_{eff} of -0.38 eV, -0.11 eV, and -2.04 eV respectively. So only the transition level of (0/3+) is meaningful for Y_i. However, such transition (0/3+) staying too high within the conduction band (CB) with position of E_V+5.76 eV, where the position of CBM is 5.594 eV higher than the VBM (i.e. E_V+5.594 eV). Meanwhile, the formation energy of Y_i is also too high with 7.57 eV in Y-rich chemical potential limit. In O-rich (Y-poor) limit, the O_i is the lowest formation energy defect with 0.67 eV in the neutral state. It has the defect reaction of $2O_i^- \rightarrow O_i^0 + O_i^{2-}$ with a negative-U_{eff} value of -2.39 eV. The TTL of (2-/0) for O_i in Y_2O_3 stays at E_V+1.58 eV. For the V_Y in the lattice, it is also a negative-U_{eff} center through the defect reactions for charge alternations as follows: $3V_Y^{2-} \rightarrow V_Y^0 + 2V_Y^{3-}$ and $V_Y^- + V_Y^{2-} \rightarrow V_Y^0 + V_Y^{3-}$ with U_{eff} value of -0.36 eV and -0.11 eV respectively. The formation energy of the neutral state V_Y^0 is 2.22 eV at the Y-poor (O-rich) limit with two nearly close TTL of (0/-) and (3-/-) for V_Y at E_V+0.89 eV and E_V+0.90 eV.

The above discussion shows that the individual intrinsic defect sites in Y_2O_3 may have either negative or positive U_{eff} for electron-lattice coupling. During the electronic transitions at the metastable state, these single individual intrinsic point defect formed are actually presented with an energy level containing single- or multi- phonons assistance for energy transfer. However, when the pair defects with a specific charge transition state, the electronic transition is actually along the closed path that the equivalent numbers of phonons are mutually offset. On the other word, it is a closed zero-phonon line for electronic transition in the host lattice independent to the environmental temperature and thermal effect, in agreement with the physical trend and satisfied the theoretical outlook by Leverenz [15]. From the transition state (0/+) of V_O to (2-/0) of O_i, it forms an electronic transition path along the zero-phonon line (ZPL), giving an emission of energy in terms of photon with 399 nm. Another transition path is from (+/2+) of V_O to either (-/0) or (3-/-) of V_Y, giving a photon emissions of about 406 nm equivalently. From the Figure 5, these closed paths are showing by following exothermic defect reactions (Eq. (7) (8), and (9)) for processing the energy transfers:

$$2V_O^0 + O_i^0 \rightarrow 2V_O^+ + O_i^{2-} + U_{eff1} \quad (7)$$

$$V_O^0 + V_Y^0 \rightarrow V_O^+ + V_Y^- + U_{eff\,2} \tag{8}$$

$$\begin{cases} 2V_O^0 + V_Y^- \rightarrow 2V_O^+ + V_Y^{3-} + U_{eff\,3} \\ 2V_O^+ + V_Y^- \rightarrow 2V_O^{2+} + V_Y^{3-} + U_{eff\,4} \end{cases} \tag{9}$$

By this calculation, we have already set the electronic transition process that only one electron is interacting with single photons. Therefore, through the results of the U_{eff} divided by experimental photon emission energy E_{em}, the numbers are approximated to the numbers of photon "virtually" to be transferred for absorption at the "activator" sites acting by intrinsic defect of the host lattice (i.e. $n_{V\text{-}photon} \approx |U_{eff}| / E_{em}$). With these numbers of "virtual photons" resonantly absorbed, another process of electronic excitations would be supported for output luminescence, which is the final emission for the persistent phosphor luminescence.

From the defect reactions shown in Eq. (7), (8), and (9), the effective correlation energies for these two-electron related defect reactions are U_{eff1}= -6.21 eV, U_{eff2}= -3.79 eV, U_{eff3}= -7.56 eV, U_{eff4}= -6.10 eV, respectively. We have E_{em}≈3.0 eV which can be either measured from our single-particle level calculations (Figure 6) or referred from the experimental observations. Accordingly, the numbers of photons given out from those closed cycle resonantly zero-photon level electronic transitions are n_1=2.07, n_2=1.26, n_3=2.52, and n_4=2.03 respectively.

Figure 6 shows the theoretical eigenvalues of the electronic structures contributed from the host lattice containing different specific native point defects, which we called single-particle levels. It contains different localized defect electronic and hole levels relative to the VBM and CBM respectively, at different intrinsic charge states. The black-line denotes the occupied electronic levels. The red-line shows the hole level or called empty state, which means an intermediate level for electron with rather short life-time. The bounded electrons can be either excited from VBM or from the localized occupied electronic states to higher levels, even the delocalized states within the CB or near the CBM. Experimentally reported two dominant and typical excitation peaks are observed during the process of UV irradiation on Y_2O_3 powder sample. One is at 288 nm (i.e. 4.31 eV for photon energy) and the other is 326 nm (i.e. 3.80 eV). The emission peak of the persistent luminescence is centering at 416 nm with typical time decay constant of 6.16 ns, found by Lin et al[83].

We firstly used the calculated single-particle levels to interpret the excitation mechanism. For the electrons excited from the VBM, the path from VBM to the localized electronic levels (E_V+4.36 eV) at V_O^0 shows the excitation wavelength of 284 nm, in a close agreement with experimentally observed peak at 288 nm. Similarly for V_O^+, a wavelength of 356 nm can be absorbed by UV irradiation from VBM to the lowest localized hole levels of V_O^+ at E_V+3.48 eV, in a good trend to the experimental 326 nm excitation peak. Another two are from VBM to the localized state given by the V_Y^0 (E_V+3.77 eV) and V_Y^- (E_V+3.76 eV) with excitation wavelength of 329 nm and 330 nm respectively. For the electrons excited from the localized levels near the VBM, the ($O_i^0 \rightarrow V_O^{2+}$) is one of the excitation center for electron starting from the E_V+0.40 eV at O_i^0 to E_V+4.84 eV at V_O^{2+} equivalent to 280 nm. Another one is the a-Fr^0 inY_2O_3 and it contributes the excitation center from electronic state at E_V+0.34 eV to E_V+3.95 eV i.e. the 318 nm. From Figure 6, we can see that the hole excitation is applicable by the UV irradiation. Note that, the external high-energy excitation can be implemented on both electrons and holes at the different traps within the same host lattice. The localized hole

staying at V_O^+ site are excited by energy scale of 453 nm (or 2.74 eV in photon energy) and drifting onto the O_i^- site with shorter life-time. This arises because the O_i^- can only be existing in the host lattice within a rather short life-time during the external excitation, due to the reaction of $2O_i^- \rightarrow O_i^0 + O_i^{2-}$ with a negative-U_{eff} value of -2.39 eV.

Then, we turn to look at the emission mechanism and energy transfer path based on the single particle levels. We see from the Figure 6 that, three types of luminescence centers are accounted for the radiative emissions of persistent luminescence. Two of them are the cooperative center and the other is the single center with triplet-type de-excitation. For the cooperative luminescence center, the excited electrons at V_O^+ (E_V+3.48 eV) site will be de-excited back to the state at O_i^{2-} (E_V+0.43 eV) corresponding to the wavelength of 407 nm. The second path is coming with shorter life-time as the transition is from V_Y^0 (E_V+3.77 eV) back to the O_i^- (E_V+0.74 eV) with wavelength of 408 nm. For the single-site emission center, it is implemented at a-Fr^0 site. The electron is being de-excited from the second localized electronic state (E_V+3.34 eV) back to the first state (E_V+0.34 eV) with equivalent wavelength of 413 nm (or 3.0 eV in photon energy).

Experimentally, the luminescence mechanism of bluish-white phosphor for Y_2O_3 is ascribed to the impurity of carbon in the host lattice. The electronic paramagnetic resonance (EPR) spectra present a strong paramagnetic signal (g=2.0050) for low temperature annealed sol-gel Y_2O_3 powder sample (550 °C) and strongest luminescence emission peak at the same temperature annealed sample. From our calculations, the doubly electronically occupied oxygen interstitial (O_i^{2-}) defect is accounted for the paramagnetic defect site due to the strong electron-lattice coupling effect dominated by negative-U_{eff} (-2.41 eV). This indicates the O_i can only exist in the host lattice with doubly electronically occupied through the reaction illustrated above. Moreover, as we analyzed from Figure 5 and Figure 6, the O_i^{2-} actually plays an intrinsic "activator" site for accommodating the electrons de-excited back from the higher excited states. Therefore, the O_i^{2-} together with V_O^+ is found to be the activator site accounting for the intrinsic bluish-white phosphor observed in sol-gel Y_2O_3 powder sample.

Meanwhile, on the other hand, the carbon (C) impurity in the Y_2O_3 lattice can be electronic inactive. The annealing temperature dependent luminescence shows the reduced emission intensity at 660 °C and quenching effect at 770 °C. This arises because the annihilation of O_i by forming C-O bond or local polymorphs of CO_2 structure. As investigated by the work of Arthur, the reaction temperature of forming C-O bond is initiated from the temperature at about 600°C and strong O-C-O double bond is formed at 800°C [84]. The single-particle level of C_i interstitial shows the localized electronic state occupying the level near the mid-gap. This blocks the electronic de-excitation path at the intrinsic activator site from V_O^+ to the O_i^{2-} sites, since the localized C_i impurity level is right sitting within the energy range between V_O^+ and O_i^{2-}.

4.5 HfO_2

HfO_2 has been also reported to have phosphorescence phenomenon for the polycrystalline, with synthesized sample recently found by Pejaković [51]. The persistent phosphorescence is found to be 2.53 eV in photon energy for the center of the emission luminescence spectra, and the luminescence time duration even reached to the scale of 150 s. The local structure of HfO_2 is similar to the polymorphs of CeO_2 we have investigated [31]. We found that the V_O, O_i and V_{Hf} are the three typical defects we need to focus on for interpreting the persistent

luminescence energy transfer mechanism. Especially, the O_i in HfO_2 lattice is coming more evident after the sintering procedure during the synthesis process.

As shown in Figure 7, it is shown that, the TTL of (0/2+) for the V_O with a transient state of (2-/0) of O_i in HfO_2 lattice can exhibit an energy release of 2.60 eV to support the further excitation and electronic at different intrinsic defect levels for emission. From our formation energy calculation, the O_i itself shows the positive-U_{eff} effect, which means the defect reaction of $2O_i^- \rightarrow O_i^0 + O_i^{2-}$ shows the transition (2-/0) only in a low probability. However, in sintering condition, the density of HfO_2 sample usually turns to be higher than ideal cubic HfO_2 lattice. Therefore, we call the (2-/0) of O_i participation in the energy transfer for phosphorescence only in a transient state, especially after a UV irradiation. In particular, we found higher sintering temperature on the sample will increase not only the density of the HfO_2 sample, but also enlarge the concentration of the metastable O_i trapped within the lattice. This deduction is consistent with experimental observation[51]. At the meanwhile, for the V_{Hf} defect site in the HfO_2 lattice can be also a candidate for the energy transition center for supporting the phosphorescence. From Figure 7, we see that the internal intra-level transition between (2-/-) of O_i and (-/0) of V_{Hf} gives the energy transition of 2.54 eV along the ZPL with offset of phonons. Therefore, both paths with energy 2.60 eV and 2.54 eV respectively will support short- and medium- range intrinsic activator center within the host lattice for intrinsic phosphorescence.

Then, which defect levels or combinations would play as the intrinsic activator for phosphorescence in HfO_2? We further discuss the result summarized in Figure 8. The blue solid line denotes the long life-time for electronic de-excitation, while the dashed line shows the shorter or transient state transitions. We confirm the V_O is an important defect center that carries the energy support the phosphorescence in HfO_2, in consistency with deduction from experiment[51]. However, in more details, combination of the single-particle levels (SPLs) of the V_O^0 with the lowest occupied localized electronic state of O_i^- gives an emission of photon energy of 2.59 eV by electronic de-excitation. Therefore, the SPL calculations show that the sole status of V_O cannot account for the phosphorescence of experimentally observed HfO_2. It is actually a combination with V_O+O_i in defect complex. Another two combinations as native self-activated in persistent luminescence are the $V_O^{2+} + V_{Hf}^0$ as well as the $V_O^{2+} + V_{Hf}^-$, giving the emission photon energies of 2.57 eV and 2.60 eV respectively. For the single defect acting as activator sites, we found that the O_i^-, V_{Hf}^0, and V_{Hf}^- can output the triplet-type electronic de-excitation from higher excited state back to the localized ground electronic states, with energies in emission of 2.53 eV, 2.62 eV and 2.59 eV respectively. These are in a good accordance with experimental measured 2.53 eV in emission spectra.

4.6 Correlation between TTLs and SPLs in energy transfer

Finally, the recombination of the electrons and holes in the solids is the most important factor determining the optical luminescence in the wide band gap semiconductor solid materials. This requires not only the specific defects that capable to donate/accept electrons but also they have relatively low formation energy and appropriate energy intervals to emit the specific energy as photons.

As shown in Figure 9, with the above discussion and analysis, we have summarized a schematic energy transfer mechanism diagram for the intrinsic or activator-doped upconverted persistent luminescence. The thermodynamic transition levels (TTLs) and single-particle levels (SPLs) by DFT calculations have been elucidated with a correlation

with non-radiative phonon emissions. This electron-lattice coupling effect through the lattice vibrations during the defect transitions is dominated by negative-U_{eff} within a closed cycle of ZPL.

5 Conclusion

In summary, we have shown how the recombination of charge carriers between different defect levels along the ZPL can lead to the persistent phosphorescence in solids. This suggests that the key driving force for this optical phenomenon is the pair electrons hopping between different charged defects with negative-U_{eff}, which is provided by the evident electron-lattice coupling effect. Such negative correlation energy will provided sustainable energy source for electron-hole further recombine in a new cycle with a specific quantum yield. This will help us to understand the intrinsic persistent luminescence from the aspect of native point defect levels.

Acknowledgement

The author BH gratefully acknowledges the support of the Natural Science Foundation of China (NSFC) for the Youth Scientist grant (Grant No.: NSFC 11504309), the initial start-up grant support from the Department General Research Fund (Dept. GRF) from ABCT in the Hong Kong Polytechnic University (PolyU), and the Early Career Scheme (ECS) fund (Grant No.: PolyU 253026/16P) from the Research Grant Council (RGC) in Hong Kong.

Figure 1.

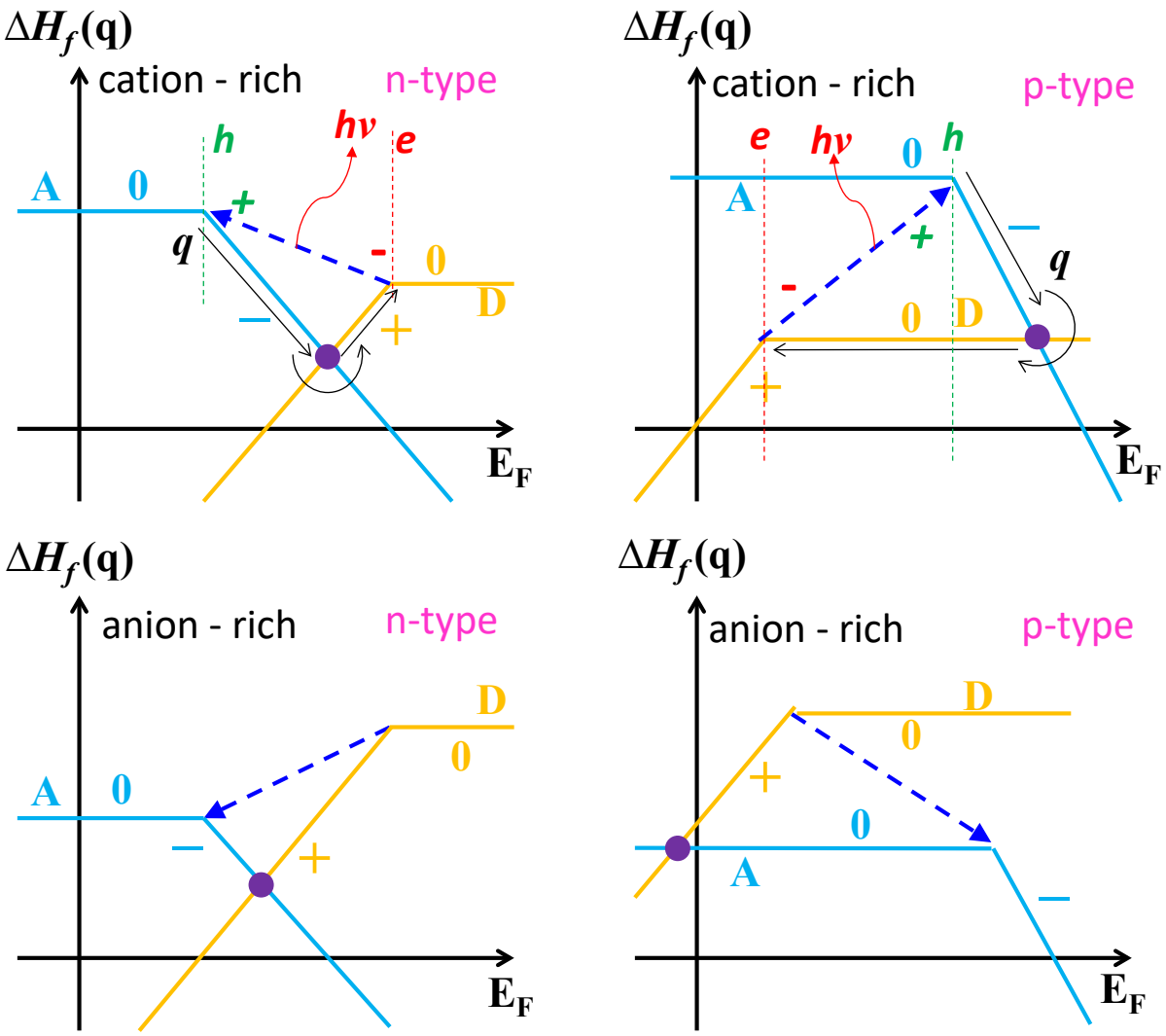

Figure 1. Schematic diagram of CAP model. $\Delta H_f(q)$ denotes the formation enthalpy of the designated intrinsic defect at the charge state q. The horizontal axis is scaled by the Fermi energy (E_F) of the electronic system of host lattice.

Figure 2.

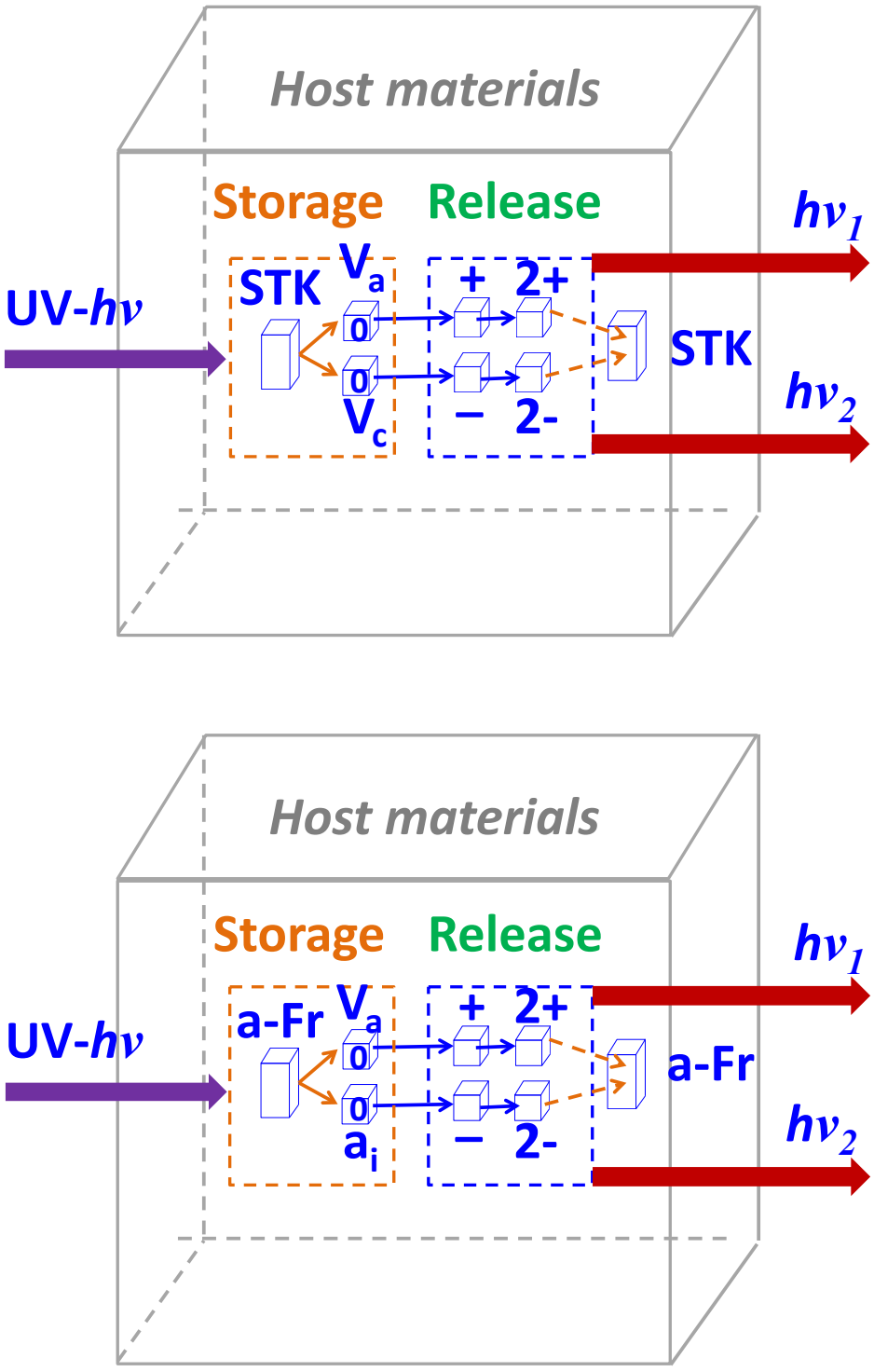

Figure 2. Persistent luminescence responsible by two types of defects one is Schottky (STK) and the other is anion Frenkel (a-Fr) pair defects.

Figure 3.

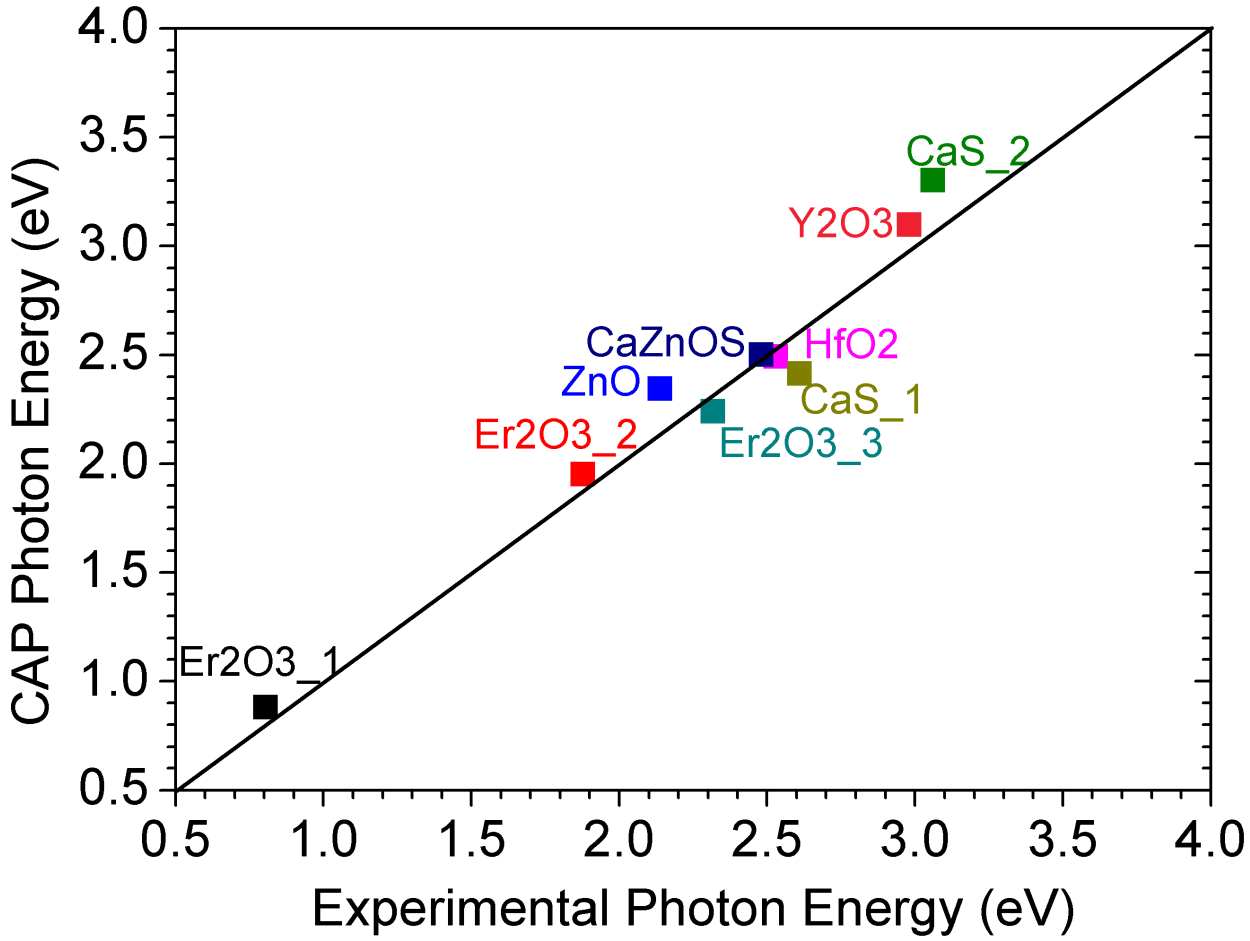

Figure 3. Comparison of the calculated photon energies by CAP model and experimental data from the measured peak center of those emission spectra during the process of intrinsic updoped persistent luminescence in phosphor solids.

Figure 4.

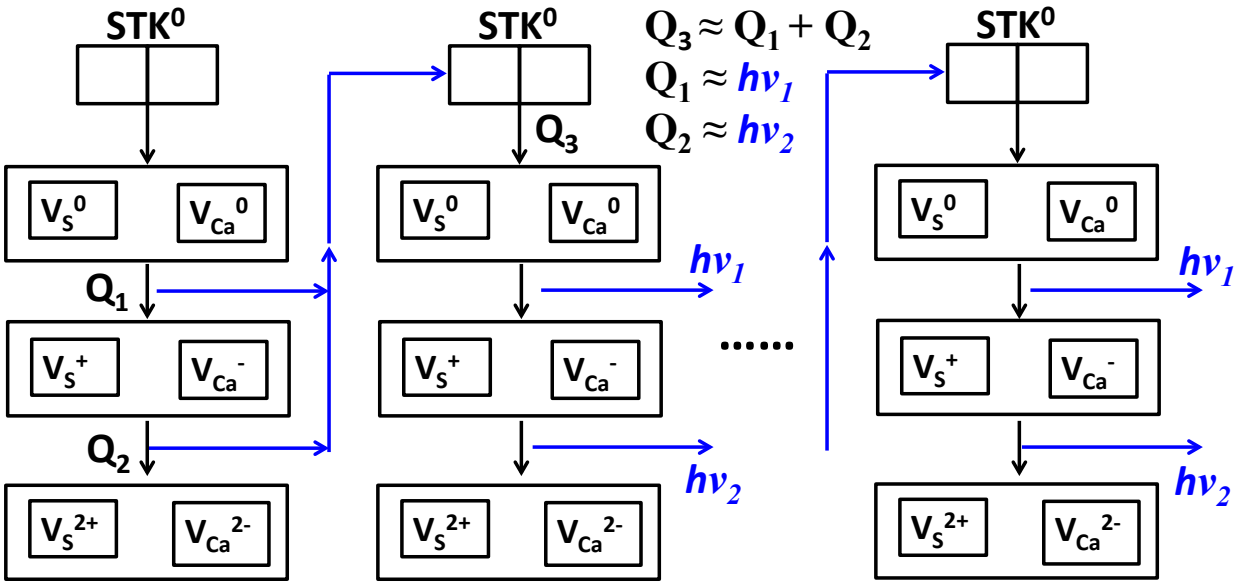

Figure 4. The schematic energy conversion cycle of ECCR in CaS (energy conversion chain reaction).

Figure 5.

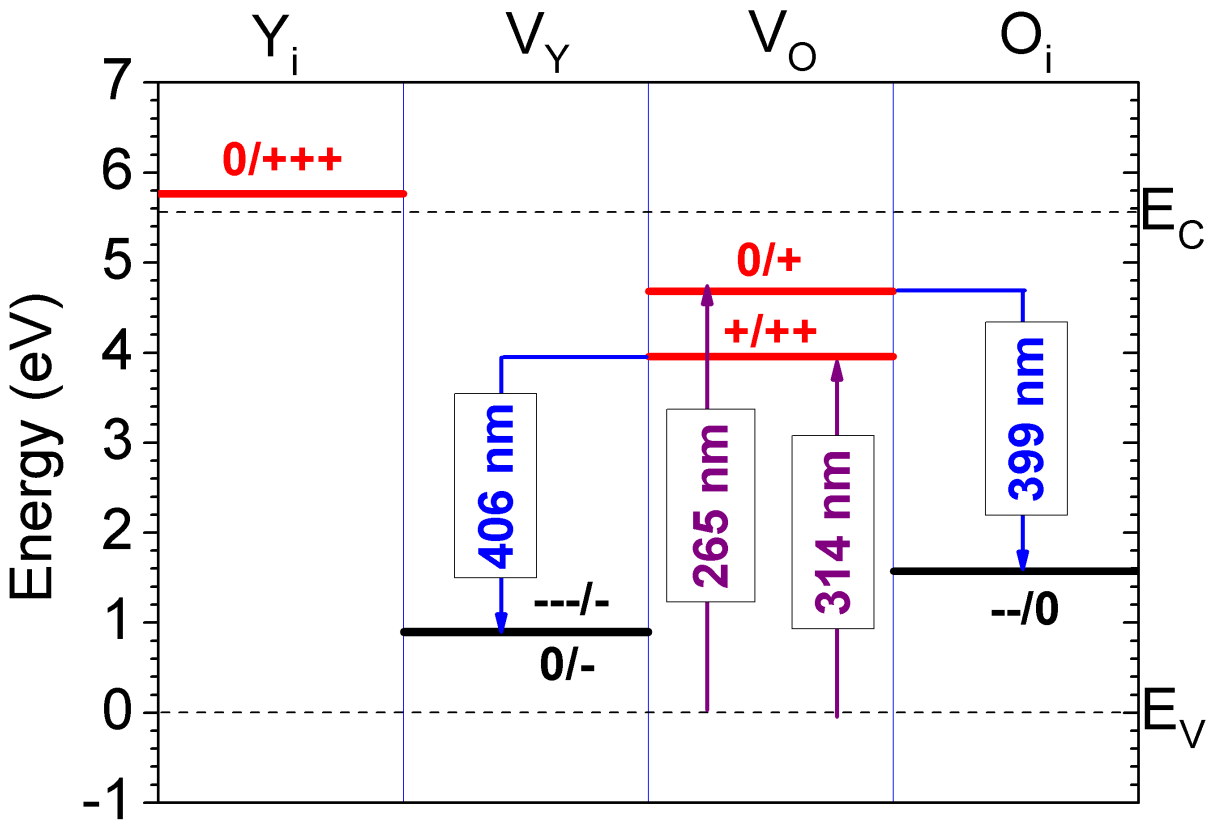

Figure 5. Summary of thermodynamic transition levels of different charge states of the intrinsic defects in cubic Y_2O_3 lattice. The red line denotes donor type transition level and black line shows the acceptor level.

Figure 6.

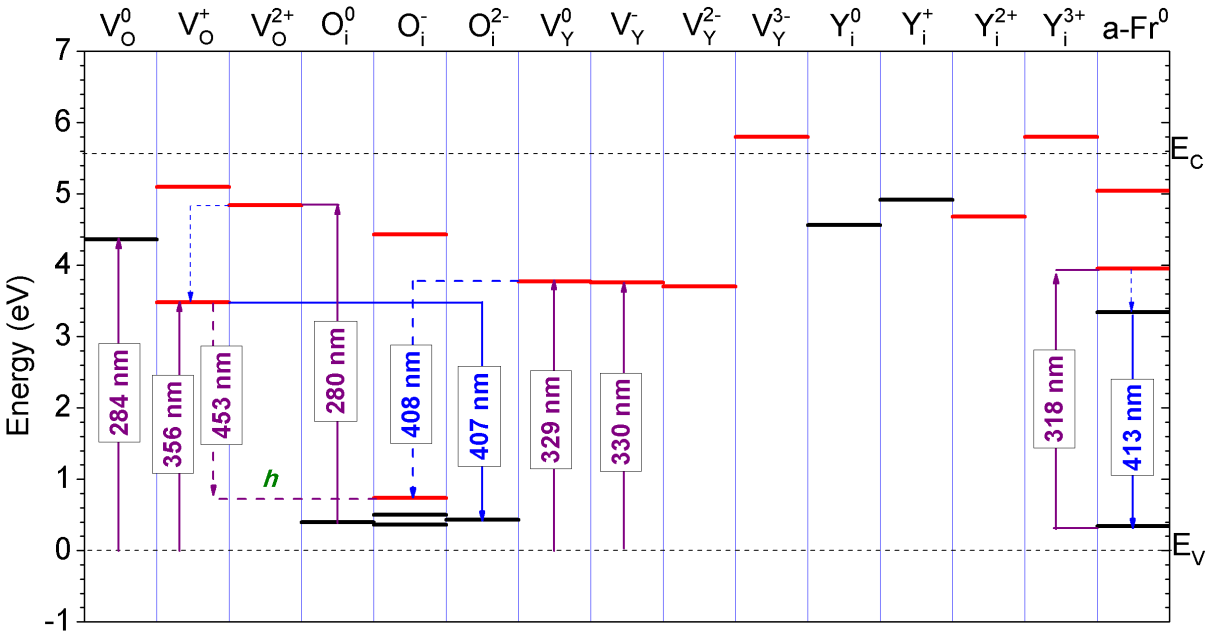

Figure 6. Summarized single-particle levels of intrinsic defects in cubic Y_2O_3 lattice with different charge states (empty states=red, filled states=black) showing the energy transport mechanism of charge carriers and energy conversions for bluish-white phosphor luminescence.

Figure 7.

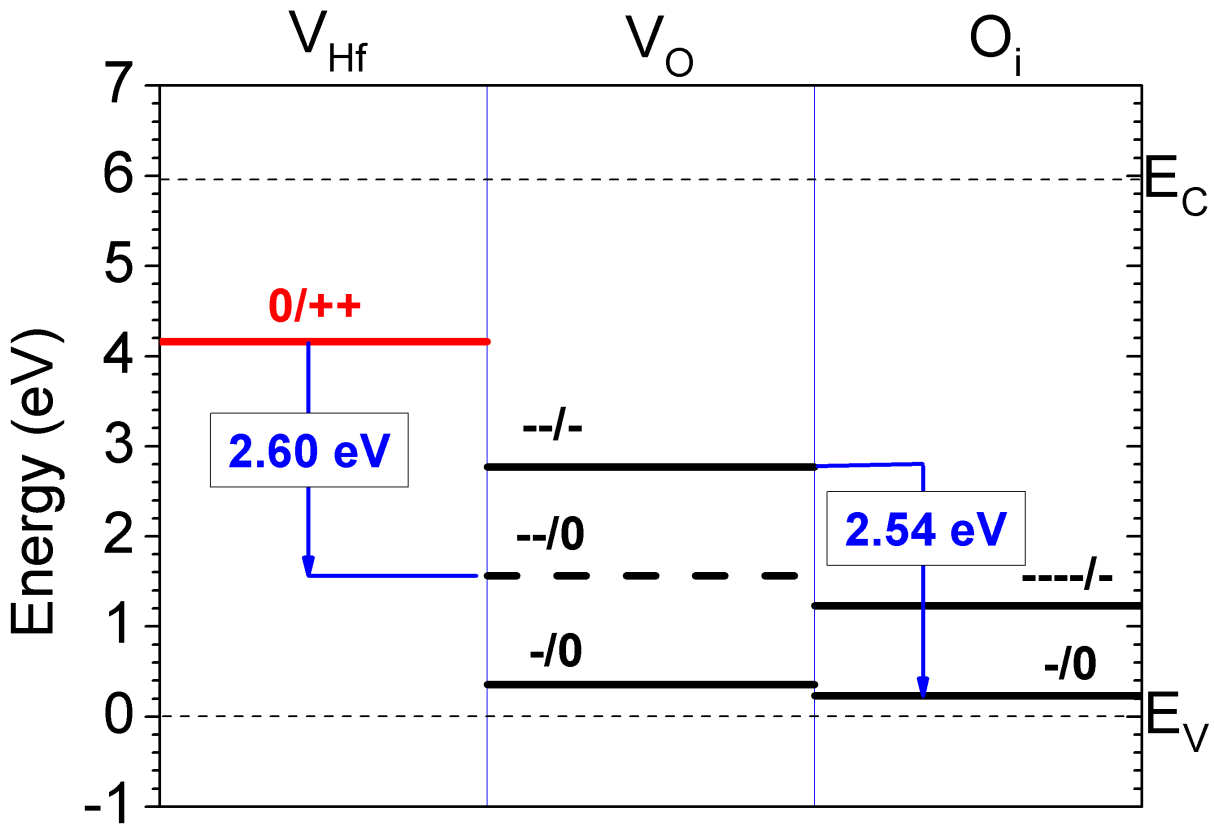

Figure 7. Summary of thermodynamic transition levels of different charge states of the intrinsic defects in cubic HfO_2 lattice. The red line denotes donor type transition level and black line shows the acceptor level. (Note, we omitted the Hf-interstitial, Hf_i, due to the rather high formation energies under both Hf-rich and O-rich chemical potential limit.)

Figure 8.

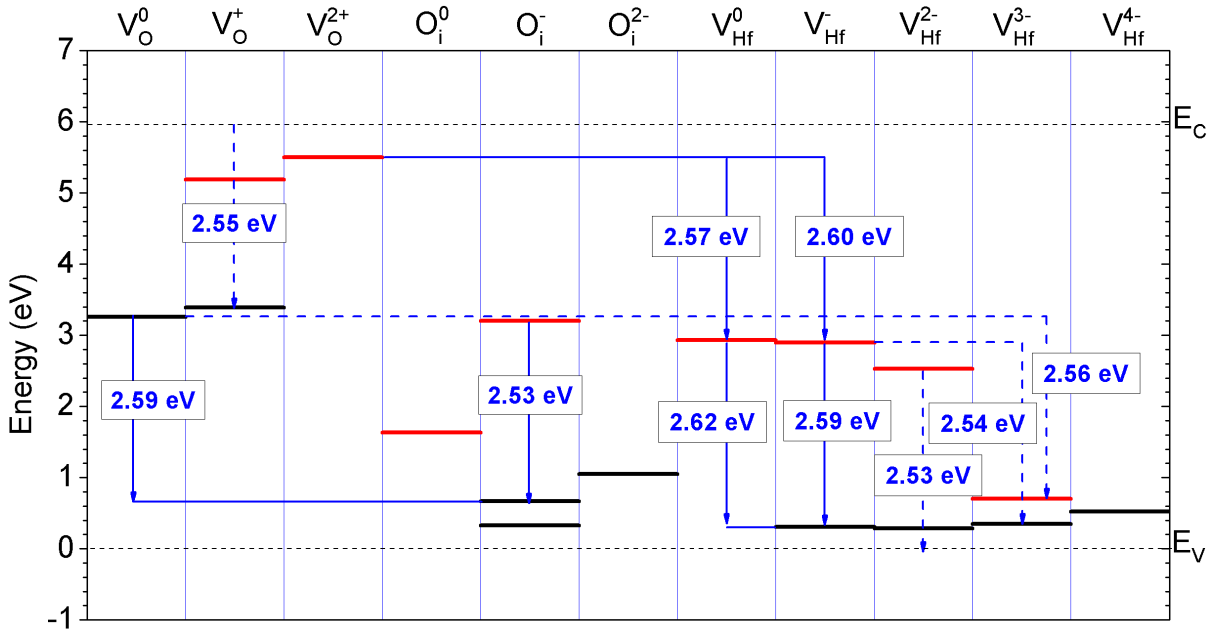

Figure 8. Summarized single-particle levels of intrinsic defects in cubic Y_2O_3 lattice with different charge states (empty states=red, filled states=black) showing the energy transport mechanism of charge carriers and energy conversions for bluish-white phosphor luminescence. (Note, we omitted the Hf-interstitial, Hf_i, due to the rather high formation energies under both Hf-rich and O-rich chemical potential limit.)

Figure 9.

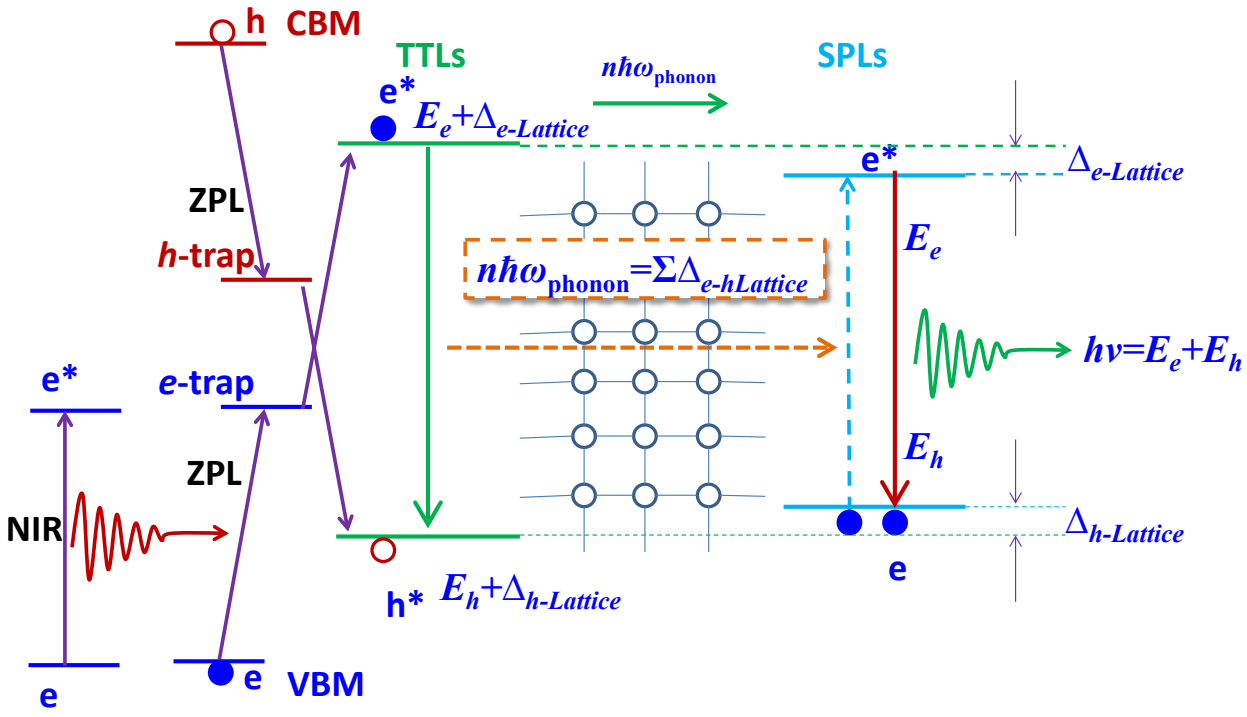

Figure 9. The schematic energy transfer mechanism diagram for upconverted persistent luminescence. The thermodynamic transition levels (TTLs) and single-particle levels (SPLs) have been elucidated with a correlation with non-radiative phonon emissions. This electron-lattice coupling effect through the lattice vibrations during the defect transitions is dominated by negative-U_{eff} within a closed cycle of ZPL.

References

[1] K. Van den Eeckhout, P. F. Smet, and D. Poelman, Materials **3**, 2536 (2010).
[2] K. Van den Eeckhout, D. Poelman, and P. Smet, Materials **6**, 2789 (2013).
[3] P. F. Smet, I. Moreels, Z. Hens, and D. Poelman, Materials **3**, 2834 (2010).
[4] J. Hölsä, Electrochem. Soc. Interf. **18**, 42 (2009).
[5] T. Aitasalo, P. Dereń, J. Hölsä, H. Jungner, J. C. Krupa, M. Lastusaari, J. Legendziewicz, J. Niittykoski, and W. Stręk, J. Solid State Chem. **171**, 114 (2003).
[6] T. Matsuzawa, Y. Aoki, N. Takeuchi, and Y. Murayama, J. Electrochem. Soc. **143**, 2670 (1996).
[7] F. Liu, W. Yan, Y.-J. Chuang, Z. Zhen, J. Xie, and Z. Pan, Scientific Reports **3**, 1554 (2013).
[8] T. Maldiney, A. Lecointre, B. Viana, A. Bessière, M. Bessodes, D. Gourier, C. Richard, and D. Scherman, J. Am. Chem. Soc. **133**, 11810 (2011).
[9] T. Maldiney, et al., Nat Mater **13**, 418 (2014).
[10] Z. Pan, Y.-Y. Lu, and F. Liu, Nat Mater **11**, 58 (2012).
[11] D. C. Rodriguez Burbano, E. M. Rodriguez, P. Dorenbos, M. Bettinelli, and J. A. Capobianco, Journal of Materials Chemistry C **2**, 228 (2014).
[12] D. C. Rodríguez Burbano, S. K. Sharma, P. Dorenbos, B. Viana, and J. A. Capobianco, Advanced Optical Materials **3**, 551 (2015).
[13] J. Wang, J. H. Hao, and P. A. Tanner, J. Lumin. **164**, 116 (2015).
[14] L. Pihlgren, et al., Opt. Mater. **36**, 1698 (2014).
[15] H. W. Leverenz, Science **109**, 183 (1949).
[16] P. K. Ghosh and B. Ray, Prog. Cryst. Growth Ch **25**, 1 (1992).
[17] D. V. Lang, J. Appl. Phys. **45**, 3023 (1974).
[18] D. V. Lang and R. A. Logan, Phys. Rev. Lett. **39**, 635 (1977).
[19] A. Janotti and C. G. Van de Walle, Phys. Rev. B **76**, 165202 (2007).
[20] B. Huang, Solid State Commun. **237–238**, 34 (2016).
[21] H. W. Leverenz, Science **157**, 414 (1967).
[22] T. Förster, Ann. Phys-berlin. **437**, 55 (1948).
[23] F. Auzel, in *Radiationless Processes*, edited by B. DiBartolo and V. Goldberg (Springer US, Boston, MA, 1980), p. 213.
[24] F. Auzel, Chem. Rev. **104**, 139 (2004).
[25] B. Huang, Inorg. Chem. **54**, 11423 (2015).
[26] B. Huang, Phys. Chem. Chem. Phys. **18**, 13564 (2016).
[27] B. Huang and J. Robertson, Phys. Rev. B **81**, 081204 (2010).
[28] B. Huang and J. Robertson, Phys. Rev. B **85**, 125305 (2012).
[29] B. Huang and J. Robertson, J. Non-cryst. Solids. **358**, 2393 (2012).
[30] B. Huang, physica status solidi (b) **252**, 431 (2015).
[31] B. Huang, R. Gillen, and J. Robertson, J. Phys. Chem. C **118**, 24248 (2014).
[32] B. Huang, Philosophical Magazine **94**, 3052 (2014).
[33] B. Huang, J. Comput. Chem. **37**, 825 (2016).
[34] S. J. Clark, J. Robertson, S. Lany, and A. Zunger, Phys. Rev. B **81**, 115311 (2010).
[35] G. Pacchioni, F. Frigoli, D. Ricci, and J. A. Weil, Phys. Rev. B **63**, 054102 (2000).
[36] S. Lany and A. Zunger, Phys. Rev. B **80**, 085202 (2009).
[37] P. W. Anderson, Physical Review **109**, 1492 (1958).
[38] P. W. Anderson, Phys. Rev. Lett. **34**, 953 (1975).
[39] N. F. Mott, E. A. Davis, and R. A. Street, Philosophical Magazine **32**, 961 (1975).
[40] R. A. Street and N. F. Mott, Phys. Rev. Lett. **35**, 1293 (1975).

[41] N. F. Mott and E. A. Davis, *Electronic Process in Non-crystalline Materials* (Clarendon Press, Oxford, 1979).
[42] N. F. Mott, Journal of Physics C: Solid State Physics **13**, 5433 (1980).
[43] E. A. Davis, Endeavour **1**, 103 (1977).
[44] G. D. Watkins, in *Advances in Solid State Physics: Plenary Lectures of the 48th Annual Meeting of the German Physical Society (DPG) and of the Divisions "Semiconductor Physics" "Metal Physics" "Low Temperature Physics" "Thermodynamics and Statistical Physics" "Thin Films" "Surface Physics" "Magnetism" "Physics of Polymers" "Molecular Physics" Münster, March 12…17, 1984*, edited by P. Grosse (Springer Berlin Heidelberg, Berlin, Heidelberg, 1984), p. 163.
[45] M. Kastner, D. Adler, and H. Fritzsche, Phys. Rev. Lett. **37**, 1504 (1976).
[46] M. Kastner, Phys. Rev. Lett. **28**, 355 (1972).
[47] G. A. Baraff, E. O. Kane, and M. Schlüter, Phys. Rev. B **21**, 5662 (1980).
[48] P. G. Baranov, N. G. Romanov, D. O. Tolmachev, C. de Mello Donegá, A. Meijerink, S. B. Orlinskii, and J. Schmidt, Jetp Lett+. **84**, 400 (2006).
[49] A. S. Gurin, N. G. Romanov, D. O. Tolmachev, and P. G. Baranov, Phys. Solid State+. **57**, 280 (2015).
[50] J. E. Stehr, S. L. Chen, N. K. Reddy, C. W. Tu, W. M. Chen, and I. A. Buyanova, Adv. Funct. Mater. **24**, 3760 (2014).
[51] D. A. Pejaković, J. Lumin. **130**, 1048 (2010).
[52] L. Jin, et al., Nano Lett. **15**, 6575 (2015).
[53] J. Wang, J. H. Hao, and P. A. Tanner, Opt. Express **19**, 11753 (2011).
[54] G.-y. Adachi and N. Imanaka, Chem. Rev. **98**, 1479 (1998).
[55] S. J. Clark, M. D. Segall, C. J. Pickard, P. J. Hasnip, M. I. J. Probert, K. Refson, and M. C. Payne, Zeitschrift Fur Kristallographie **220**, 567 (2005).
[56] C. J. Pickard, B. Winkler, R. K. Chen, M. C. Payne, M. H. Lee, J. S. Lin, J. A. White, V. Milman, and D. Vanderbilt, Phys. Rev. Lett. **85**, 5122 (2000).
[57] T. Zacherle, A. Schriever, R. A. De Souza, and M. Martin, Phys. Rev. B **87**, 134104 (2013).
[58] P. R. L. Keating, D. O. Scanlon, B. J. Morgan, N. M. Galea, and G. W. Watson, J. Phys. Chem. C **116**, 2443 (2011).
[59] B. Huang, Solid State Commun. **230**, 49 (2016).
[60] P. J. Hasnip and C. J. Pickard, Comput. Phys. Commun. **174**, 24 (2006).
[61] K. Laasonen, A. Pasquarello, R. Car, C. Lee, and D. Vanderbilt, Phys. Rev. B **47**, 10142 (1993).
[62] A. M. Rappe, K. M. Rabe, E. Kaxiras, and J. D. Joannopoulos, Phys. Rev. B **41**, 1227 (1990).
[63] L. Kleinman and D. M. Bylander, Phys. Rev. Lett. **48**, 1425 (1982).
[64] S. G. Louie, S. Froyen, and M. L. Cohen, Phys. Rev. B **26**, 1738 (1982).
[65] I. Grinberg, N. J. Ramer, and A. M. Rappe, Phys. Rev. B **62**, 2311 (2000).
[66] N. Marzari, D. Vanderbilt, and M. C. Payne, Phys. Rev. Lett. **79**, 1337 (1997).
[67] M. I. J. Probert and M. C. Payne, Phys. Rev. B **67**, 075204 (2003).
[68] I. A. Vladimir, F. Aryasetiawan, and A. I. Lichtenstein, J. Phys. Condens. Matter **9**, 767 (1997).
[69] S. Lany and A. Zunger, Phys. Rev. B **80**, 085202 (2009).
[70] S. Lany and A. Zunger, Phys. Rev. B **81**, 205209 (2010).
[71] B. J. Morgan and G. W. Watson, J. Phys. Chem. C **114**, 2321 (2010).
[72] S. Lany and A. Zunger, Phys. Rev. B **78**, 235104 (2008).
[73] B. Huang, Phys. Chem. Chem. Phys. **18**, 25946 (2016).

[74] B. Huang, D. Peng, and C. Pan, Phys. Chem. Chem. Phys. **19**, 1190 (2017).
[75] Q. Yang, W. Wang, S. Xu, and Z. L. Wang, Nano Lett. **11**, 4012 (2011).
[76] Q. Yang, Y. Liu, C. Pan, J. Chen, X. Wen, and Z. L. Wang, Nano Lett. **13**, 607 (2013).
[77] J. Zhang, Sun, Yin, Su, Liao, and Yan, Chem. Mater. **14**, 4172 (2002).
[78] K. Vanheusden, W. L. Warren, C. H. Seager, D. R. Tallant, J. A. Voigt, and B. E. Gnade, J. Appl. Phys. **79**, 7983 (1996).
[79] S. A. Studenikin, N. Golego, and M. Cocivera, J. Appl. Phys. **84**, 2287 (1998).
[80] L. Spanhel and M. A. Anderson, J. Am. Chem. Soc. **113**, 2826 (1991).
[81] S. J. Clark and J. Robertson, physica status solidi (b) **248**, 537 (2011).
[82] Y. N. Chen, S. J. Xu, C. C. Zheng, J. Q. Ning, F. C. C. Ling, W. Anwand, G. Brauer, and W. Skorupa, Appl. Phys. Lett. **105**, 041912 (2014).
[83] C. Lin, C. Zhang, and J. Lin, J. Lumin. **129**, 1469 (2009).
[84] J. R. Arthur, Transactions of the Faraday Society **47**, 164 (1951).

TOC

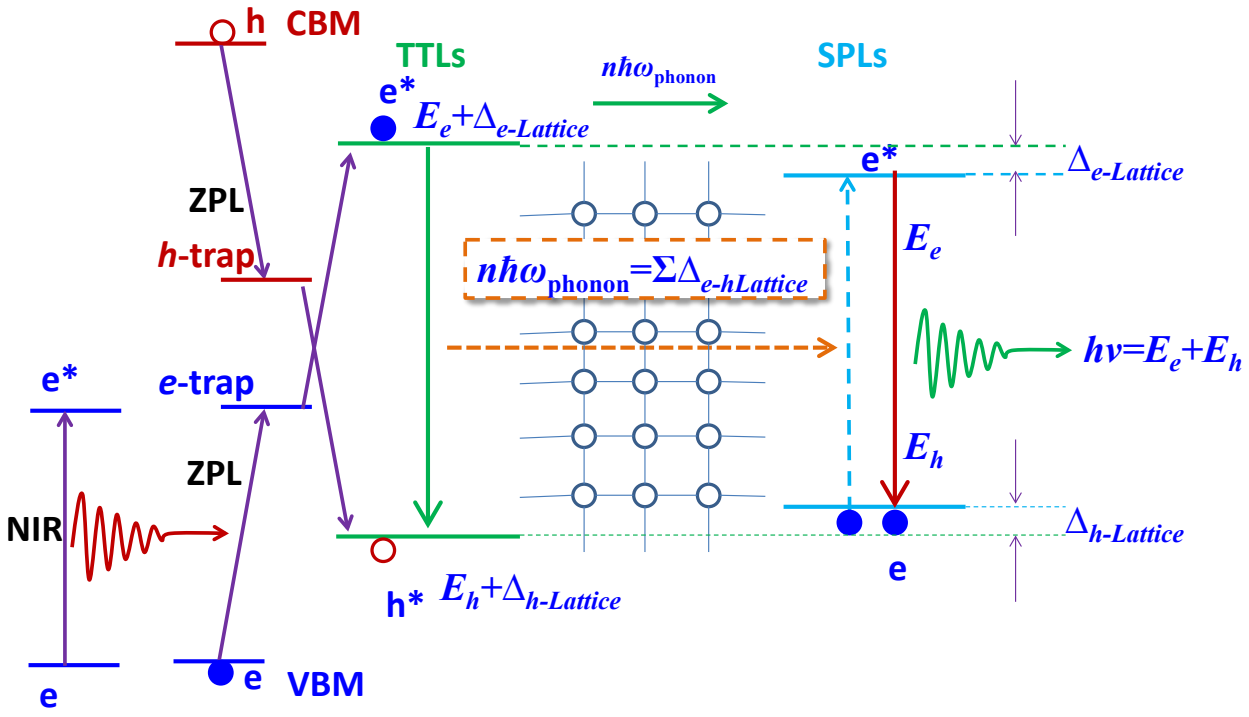

Synopsis (20 words)

The energy transfer mechanism for persistent luminescence. The thermodynamic transition levels (TTLs) and single-particle levels (SPLs) are correlated with phonons.